# What drives the Quasar Main Sequence?

Swayamtrupta Panda[1·2], Bożena Czerny[1·2],
Conor Wildy[1] and Marzena Śniegowska[1·3]

1. Center for Theoretical Physics, Al. Lotników 32/46, 02–668 Warsaw, Poland
2. Nicolaus Copernicus Astronomical Center, ul. Bartycka 18, 00–716 Warsaw, Poland
3. Warsaw University Observatory, Al. Ujazdowskie 4, 00-478 Warsaw, Poland

Eigenvector 1 (EV1), which is a combination of 13 properties from the Principal Component Analysis (PCA), was found to be the dominant component behind the significant correlations for the measured parameters in quasar spectra (Boroson & Green 1992). The parameter $R_{\rm FeII}$, which strongly correlates to the EV1, is the FeII strength, defined to be the ratio of the equivalent width of FeII to the equivalent width of H$\beta$. This allows construction of a quasar main sequence analogous to the stellar properties driven HR diagram (Sulentic et al. 2001). We try to find the main driver behind the EV1 among the basic (theoretically motivated) parameters of an active nucleus (Eddington ratio, black hole mass, accretion rate, spin, and viewing angle). Based on theoretical modeling using the photoionization code CLOUDY (Ferland et al. 2013), we test the hypothesis that the physical driver of EV1 is the maximum of the accretion disk temperature ($T_{\rm BBB}$), reflected in the shape of the spectral energy distribution (SED). We have assumed that both H$\beta$ and FeII emission come from the Broad Line Region, which is represented as a constant density cloud in a plane-parallel geometry. We test the effect of changing Eddington ratio on the $R_{\rm FeII} - T_{\rm BBB}$ trends with varying mean hydrogen densities. We also test the effect of adding microturbulence that affect the line intensities on the overall $R_{\rm FeII} - T_{\rm BBB}$ picture.

## 1 Introduction

It has been over two decades of searching for a physically motivated parameter guiding the main sequence for quasars (Boroson & Green 1992; Sulentic et al. 2000, 2002, 2007; Yip et al. 2004; Shen & Ho 2014; Sun & Shen 2015). Using principal component analysis, it has been found that this sequence is driven mostly by the Eddington ratio (Boroson & Green 1992; Sulentic et al. 2000; Shen & Ho 2014) but also with the additional effect of the black hole mass, viewing angle and the intrinsic absorption (Shen & Ho 2014; Sulentic et al. 2000; Kuraszkiewicz et al. 2009). Eigenvector 1 (EV1) is dominated by the anti-correlation between the FeII optical emission and [OIII] line which itself accounts for 30% of the total variance. The parameter $R_{\rm FeII}$, which strongly correlates to the EV1, is the FeII strength, defined to be the ratio of the equivalent width of FeII to the equivalent width of H$\beta$. We postulate that the true driver behind the $\rm R_{FeII}$ is the maximum of the temperature in a multicolor accretion disk which is also the basic parameter determining the broad band shape of the quasar continuum emission. The prescription in detail is provided in Panda et al. (2017a) and Panda et al. (2017).

## 2 Results and Discussions

In Panda et al. (2017), we found that by changing the basic assumption from "*considering a constant bolometric luminosity*" (Method 1) to "*considering a constant Eddington ratio*" (Method 2), along with the presence of the hard X-ray power law and using the observational relation between UV and X-ray luminosities from Lusso & Risaliti (2017) to determine the broad band spectral index, $\alpha_{\rm ox}$, changed the behaviour of the trend between $R_{\rm FeII} - T_{\rm BBB}$ from monotonically declining to monotonically rising in the considered range of maximum of the disk temperatures $[5 \times 10^4\ {\rm K}, 5 \times 10^5\ {\rm K}]$. Additionally we found that, with increase in mean hydrogen density ($n_{\rm H}$) of the single-cloud (going from $10^{10}$ cm$^{-3}$ to $10^{11}$ cm$^{-3}$), the FeII strength i.e. $R_{\rm FeII}$ goes down by a factor 2. In other words, the FeII emission gets suppressed as we increase the mean hydrogen density. The dependence on the change of the Eddington ratio is not as significant as thought. Fig. 1(a,b) shows the effect of changing the Eddington ratio on the $R_{\rm FeII} - T_{\rm BBB}$. In Fig. 1(a), we show the $R_{\rm FeII} - T_{\rm BBB}$ trends by changing the Eddington ratio from 0.1 to 1. At lower temperatures ($T_{\rm BBB} < 2.24 \times 10^4$ K) we see again a rise in the value of $R_{\rm FeII}$ for both cases. This rise is due to the rise in the value of the $\alpha_{\rm ox}$ for $T_{\rm BBB} < 2.24 \times 10^4$ K as illustrated in Fig. 2(a).

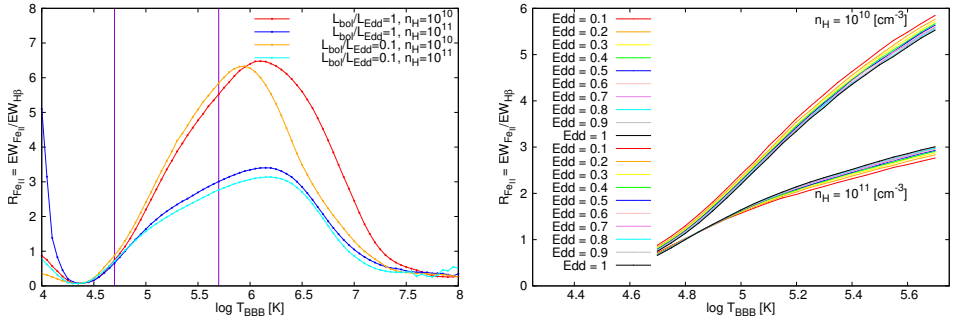


Fig. 1: (a) Comparing $R_{\rm FeII} - T_{\rm BBB}$ trends between two cases of Eddington ratio $\left(\frac{L_{\rm bol}}{L_{\rm Edd}=0.1\ \&\ 1}\right)$. The vertical red lines specify the maximum disk temperatures for which the derived black hole masses lie in the range $[6.06 \times 10^5\ M_\odot, 6.06 \times 10^9\ M_\odot]$; (b) Comparing $R_{\rm FeII} - T_{\rm BBB}$ trends for 10 consecutive cases of change in Eddington ratio (mentioned here as Edd) in the range [0.1, 1] within the considered maximum disk temperature range $[5 \times 10^4\ {\rm K} - 5 \times 10^5\ {\rm K}]$. For all of the cases, we vary the mean hydrogen density ($n_{\rm H} = 10^{10}$ cm$^{-3}$ & $10^{11}$ cm$^{-3}$).

In Fig. 1(b), we zoom the simulations into the considered range of $T_{\rm BBB}$ and show the $R_{\rm FeII} - T_{\rm BBB}$ trends by varying the Eddington ratio within the range [0.1,1] with a step size of 0.1. We test these cases again by varying the $n_{\rm H}$ as in Fig. 1(a). Although there is not a strong dependence of $R_{\rm FeII}$ on the change in Eddington ratio, for the lower $n_{\rm H}$ i.e. $10^{10}$ cm$^{-3}$, the trends rise uniformly with the trend corresponding to the lowest Eddington ratio case has the maximum value for $R_{\rm FeII} = 5.847$. But in the higher $n_{\rm H}$ case, the trends converge at $\log T_{\rm BBB} = 4.899$, but then diverge. After the divergence the slope of trend corresponding to the highest Eddington ratio case (=1.0) is the highest and has the maximum value for $R_{\rm FeII} = 3.007$.

We also include microturbulence to test its effect on the existing $R_{\rm FeII} - T_{\rm BBB}$ trends. We consider five distinct scenarios ($v_{\rm turb} = 10, 20, 30, 50, 100\,{\rm km\,s^{-1}}$) and plot in Fig. 2(b), the subsequent $R_{\rm FeII} - T_{\rm BBB}$ trends obtained alongside the existing trend (without microturbulence). We currently limit to $n_{\rm H} = 10^{11}\,{\rm cm^{-3}}$, the column density $N_{\rm H} = 10^{24}\,{\rm cm^{-2}}$. The maximum of the peak value of $R_{\rm FeII}$ is obtained for the original case without any microturbulence. The peak of $R_{\rm FeII}$ subsequently drops to its lowest value for $v_{\rm turb} = 10\,{\rm km\,s^{-1}}$ and rises as the turbulent velocity is increased till $v_{\rm turb} = 100\,{\rm km\,s^{-1}}$ falling short of the original peak $R_{\rm FeII}$. The peak values mentioned are that of the maximum value obtained within the temperature range $2.24 \times 10^4$ K $-$ $10^8$ K as the rise below $2.24 \times 10^4$ K is as explained above due to the effect of $\alpha_{\rm ox}$. But the temperature corresponding to the peak value of $R_{\rm FeII}$ shifts towards higher temperatures with increasing turbulent velocity.

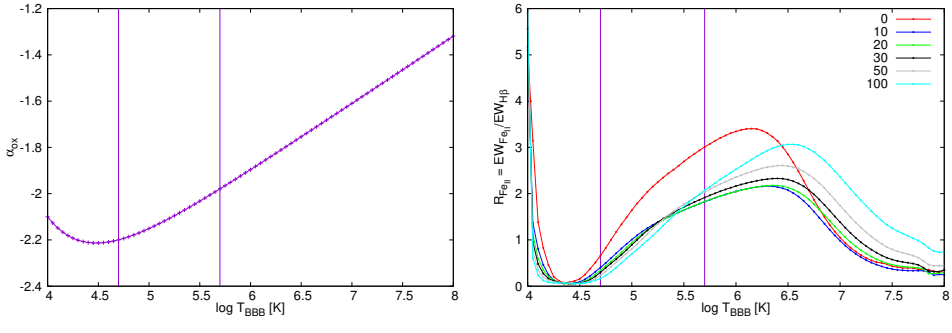


Fig. 2: (a) The changing broad band spectral index, $\alpha_{\rm ox}$ with increasing disk temperature ($T_{\rm BBB}$) . The trend is almost linear in the considered temperature range shown by the vertical red lines. (b) Comparing $R_{\rm FeII} - T_{\rm BBB}$ trends for six different cases of turbulent velocity ($v_{\rm turb} = 0, 10, 20, 30, 50, 100)\,{\rm km\,s^{-1}}$ at $n_{\rm H} = 10^{11}\,{\rm cm^{-3}}$, $N_{\rm H} = 10^{24}\,{\rm cm^{-2}}$.

With this single-cloud under constant density approximation and incorporating Method 2, we have shown that our hypothesis – the $T_{\rm BBB}$ is the driver of the Quasar Main Sequence – is justified.

*Acknowledgements.* The project is supported by the Polish National Science Center grant No. 2015/17/B/ST9/03436/.

## References

Boroson, T. A., Green, R. F., *ApJS* **80**, 109 (1992)

Ferland, G. J., et al., *RMxAA* **49**, 137 (2013)

Kuraszkiewicz, J., et al., *ApJ* **692**, 1180 (2009)

Lusso, E., Risaliti, G., *A&A* **602**, A79 (2017)

Panda, S., Czerny, B., Wildy, C., *Frontiers in Astronomy and Space Sciences* **4**, 33 (2017a), URL `https://www.frontiersin.org/article/10.3389/fspas.2017.00033`

Panda, S., Czerny, B., Wildy, C., Śniegowska, M., *ArXiv e-prints* (2017)

Shen, Y., Ho, L. C., *Nature* **513**, 210 (2014)

Sulentic, J. W., Calvani, M., Marziani, P., *The Messenger* **104**, 25 (2001)

Sulentic, J. W., Dultzin-Hacyan, D., Marziani, P., in S. Kurtz (ed.) Revista Mexicana de Astronomia y Astrofisica Conference Series, *Revista Mexicana de Astronomia y Astrofisica, vol. 27*, volume 28, 83–88 (2007)

Sulentic, J. W., Zwitter, T., Marziani, P., Dultzin-Hacyan, D., *ApJl* **536**, L5 (2000)

Sulentic, J. W., et al., *ApJl* **566**, L71 (2002)

Sun, J., Shen, Y., *ApJl* **804**, L15 (2015)

Yip, C. W., et al., *AJ* **128**, 2603 (2004)